

Article

Influence of the Hot-Pressing Rate on the Interface Feature and Mechanical Properties of Mg/Al Composite Plates

Chuande Guo, Bo Song ^{*}, Shijun Tan, Haohua Xu, Meng Wang, Tingting Liu ^{*}, Ning Guo 
and Shengfeng Guo 

School of Materials and Energy, Southwest University, Chongqing 400715, China; as1062728115@email.swu.edu.cn (C.G.); tsj123456@email.swu.edu.cn (S.T.); x18729766940@email.swu.edu.cn (H.X.); meng.wang@tytatest.com (M.W.); whc34@swu.edu.cn (N.G.); sfguo@swu.edu.cn (S.G.)

* Correspondence: bosong@swu.edu.cn (B.S.); tliu@swu.edu.cn (T.L.)

Abstract: In this work, Mg/Al composite plates were prepared by direct hot pressing under atmospheric conditions. The impacts of the strain rate (from $3.3 \times 10^{-4} \text{ s}^{-1}$ to $1.0 \times 10^{-2} \text{ s}^{-1}$) on the interface and bonding strength were investigated. Results showed that Mg/Al composite plates can be successfully fabricated by hot pressing with a 40% strain at 350 °C. The strain rate will largely affect the interfacial bonding quality and the structure of the interface. As the strain rate decreases, the thickness of the diffusion layer at the interface becomes thicker, and the composition of the interface gradually changes from a mixed zone of Mg₁₇Al₁₂ and Mg₂Al₃ to two single-phase zones. In all samples, the Mg₂Al₃ phase layer at the interface tends to exhibit brittle fracture during shear. When the strain rate of the hot pressing reduces to $3.3 \times 10^{-4} \text{ s}^{-1}$, the single-phase zone of Mg₂Al₃ at the interface breaks up. In the present work, the Mg/Al plate hot pressed at a strain rate of $1.0 \times 10^{-3} \text{ s}^{-1}$ demonstrates the highest shear strength.

Keywords: Mg/Al; laminated metal composites; hot pressing; interface



Citation: Guo, C.; Song, B.; Tan, S.; Xu, H.; Wang, M.; Liu, T.; Guo, N.; Guo, S. Influence of the Hot-Pressing Rate on the Interface Feature and Mechanical Properties of Mg/Al Composite Plates. *Metals* **2024**, *14*, 23. <https://doi.org/10.3390/met14010023>

Academic Editor: Guido Di Bella

Received: 21 November 2023

Revised: 14 December 2023

Accepted: 19 December 2023

Published: 24 December 2023



Copyright: © 2023 by the authors. Licensee MDPI, Basel, Switzerland. This article is an open access article distributed under the terms and conditions of the Creative Commons Attribution (CC BY) license (<https://creativecommons.org/licenses/by/4.0/>).

1. Introduction

The development of multi-metal hybrid composite materials has shown promising results in enhancing material properties like strength, plasticity, stiffness, impact performance, and wear resistance. In recent years, scholars have extensively studied various multi-layer composite materials, including Ni-Ti [1], Al-Cu [2,3], Cu-Ni [3], Mg-Al [4,5], and Ti-Al [6]. Among them, the layered metal composite materials involving Mg-Al have received significant attention in the field [7–11].

Magnesium and its alloys are known to be one of the lightest metals [12]. As structural materials, they offer many advantages, such as low density, high specific strength, high specific stiffness, good damping properties, and excellent electromagnetic shielding properties. However, their widespread use is limited because their resistance to corrosion and plasticity at room temperature is not excellent [13]. On the contrary, aluminum and its alloys offer better corrosion resistance and formability [14]. Therefore, high hopes have been placed on magnesium/aluminum layered composites to unify the advantages of magnesium and aluminum alloys and open up new possibilities for their applications [15].

Different methods have been utilized to fabricate Mg/Al laminated metal composites (LMCs) [16–18]. Guan et al. [16] used a compound casting method to fabricate Mg/Al LMCs. Some welding techniques (e.g., explosive welding, vacuum diffusion welding, etc.) have also been used to prepare the laminated composite plates [19]. In addition, several plastic processing techniques (e.g., extrusion, forging and rolling, etc.) have been used to develop wrought Mg/Al composite plates [20]. Compared to other technologies, plastic processing brings a plethora of benefits, such as refining the microstructure and increasing productivity. Hot pressing is another crucial technique in plastic processing, known for its flexibility,

efficiency, and controllability in producing small-size parts [21]. However, relatively few studies have been conducted on the use of hot pressing to prepare Mg/Al composite plates. In the previous report, hot pressing usually requires higher temperatures and longer heat treatment times to realize effective metallurgical bonding [22]. Additionally, a high plastic strain was performed to expose more new surfaces to facilitate inter-diffusion and metallurgical bonding under atmospheric conditions [23,24]. However, a comprehensive investigation into the effects of processing parameters on the interface and mechanical properties of hot-pressed Mg/Al plates is still lacking.

For plastic processing techniques, the strain rate is an important processing parameter [25]. It is well known that high strain rates can increase productivity, while low strain rates increase the time for interfacial diffusion [26]. Nevertheless, up until this point, no studies have been conducted to investigate the impact of the hot-pressing rate on the thickness and structure of the diffusion layer, as well as the bond strength of Mg/Al composite sheets. In this study, Mg/Al LMCs were efficiently produced at a temperature of 350 °C under varying strain rates ($1.0 \times 10^{-2} \text{ s}^{-1}$, $2.0 \times 10^{-3} \text{ s}^{-1}$, $1.0 \times 10^{-3} \text{ s}^{-1}$, $3.3 \times 10^{-4} \text{ s}^{-1}$). The impact of different strain rates on the interface structure and shear strength was systematically examined.

2. Materials and Methods

In this work, a AZ31 magnesium alloy plate (3 mm × 15 mm × 15 mm) and a 1060 aluminum alloy plate (3 mm × 15 mm × 15 mm) were used as raw materials. Prior to hot pressing, the surfaces of the samples were carefully polished with sandpaper to eliminate the surface oxides. Subsequently, the samples were subjected to ultrasonic cleaning with ethanol for a period of 10 min, followed by rapid drying with cold air. The treated 1060 aluminum alloy plate was stacked on top of the AZ31 magnesium alloy plate. Hot pressing was carried out at 350 °C with a deformation rate of 40% under different strain rates (from $1.0 \times 10^{-2} \text{ s}^{-1}$ to $3.3 \times 10^{-4} \text{ s}^{-1}$) to manufacture Mg/Al LMCs. The hot-press equipment used a universal testing machine and a high and low temperature test chamber (WGDN-7350M, LiShi (Shanghai) Instruments Co., Ltd., Shanghai, China), with a temperature range of −70 °C to +350 °C. Before hot pressing, the two hot-pressing molds were first heated to 350 °C. The molds were then placed in contact with the Mg/Al sample and held for 10 min to allow the heating of the sample. Finally, the assembled Mg/Al composite sheets are hot-pressed to a strain of 40% at various strain rates. In order to better understand the deformation process, the strain (%) may be replaced with logarithmic strain $\epsilon = \ln(h/h_0)$, where h is the final thickness and h_0 is the initial thickness. For the present hot-pressing process, the logarithmic strain is ~0.51. Table 1 displays the detailed processing parameters of different samples.

Table 1. Hot-pressing parameters of different specimens.

Sample	Thickness Reduction	Strain Rate	Hot-Pressing Time
P1	40%	$1.0 \times 10^{-2} \text{ s}^{-1}$	1 min
P2	40%	$2.0 \times 10^{-3} \text{ s}^{-1}$	5 min
P3	40%	$1.0 \times 10^{-3} \text{ s}^{-1}$	10 min
P4	40%	$3.3 \times 10^{-4} \text{ s}^{-1}$	30 min

The interface structure was examined using a scanning electron microscope (SEM, JSM-6610, JEOL, Tokyo, Japan) operating at 20 kV. The chemical element concentration was assessed using energy-dispersive spectroscopy (EDS, JSM-6610, JEOL, Tokyo, Japan). The samples used for SEM are ground with 400# to 4000# silicon carbide paper, and then the samples are put into an ultrasonic cleaner for cleaning for 10 min. Shear tests were carried out on an LD26.105 material test machine (LiShi (Shanghai) Instruments Co., Ltd., Shanghai, China) at a loading speed of 1 N/s (using the ASTM D4896 standard) [27]. The fractured surfaces of the failed LMCs from the shear test were examined by SEM and X-ray diffraction (XRD, Shimadzu, MAXima XRD-7000, Kyoto, Japan).

3. Results and Discussion

3.1. The Impact of the Strain Rate on Diffusion Thickness

Figure 1 displays the SEM images capturing the interfaces of diverse Mg/Al composite sheets. This refers to the present hot-pressing technique with a thickness reduction of 40% at 350 °C, which can generate a good connection between 1060 and AZ31. According to reports [28,29], the bonding of the composite sheets relies on two crucial factors: the deformation temperature and the amount of strain. Diffusion is slower at low temperatures, thus affecting the quality of the metallurgical bond. When the strain amount falls below a critical value, the oxide layer present on the metal surface proves challenging to break, thus restricting the exposure of fresh metal. As a result, the composite plates are unable to generate strong metallurgical bonding. Liu et al. [10] discovered that the roll bonding threshold strain for the AZ31/1060 composite sheets is 20%. Thus, a thickness reduction of 40% at 350 °C can generate an effective metallurgical bond. Additionally, it has been observed that the strain rate exerts a significant impact on the characteristics of the interface. When subjected to hot pressing with strain rates varying from $1.0 \times 10^{-3} \text{ s}^{-1}$ to $1.0 \times 10^{-2} \text{ s}^{-1}$, a flawless interface layer forms, characterized by the absence of cracks and pores. After the strain rate is further reduced to $3.3 \times 10^{-4} \text{ s}^{-1}$, the interface layer undergoes fragmentation. Moreover, numerous white particles can be found on the entire cross-section. EDS analysis indicates that these particles may be rich in O, C, Si, Mn, etc. It indicates that some particles may be the polishing residues from SiC sandpapers.

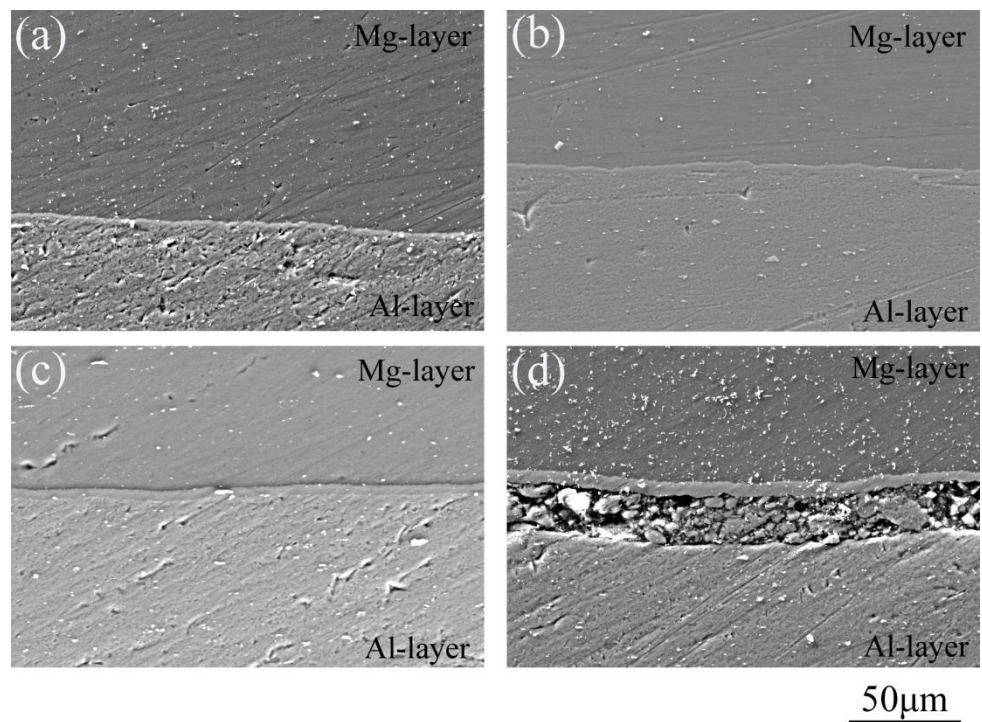


Figure 1. SEM images capturing Mg/Al sheets fabricated through hot pressing under varying strain rates: (a) $1.0 \times 10^{-2} \text{ s}^{-1}$, (b) $2.0 \times 10^{-3} \text{ s}^{-1}$, (c) $1.0 \times 10^{-3} \text{ s}^{-1}$, (d) $3.3 \times 10^{-4} \text{ s}^{-1}$.

In order to delve deeper into the interface characteristics, Figure 2 presents magnified SEM images along with area-scanning images. It is evident that a distinct interface layer is visibly formed between AZ31 and 1060 during the hot-pressing process. The element Mg and element Al exhibit full inter-diffusion across the entire interface. This further proves that direct hot pressing in an atmospheric environment can generate an effective bond at the interface of AZ31 and 1060. As the strain rate decreases, the thickness of the inter-diffusion layer gradually increases. Figure 2d shows that the interface layer of the P4 sample is obviously broken. This is primarily the underlying cause for the presence of

numerous cracks and pores on the interface of the P4 sample. As the strain rate decreases, a noticeable trend emerges: the diffusion layer progressively thickens. The element line-scanning spectrums of different samples are shown in Figure 3. Due to the occurrence of inter-diffusion, the concentrations of Mg and Al show a gradual change at the interface. Within this diffusion layer, the concentration of Al decreased from the Al alloy side to the Mg alloy side, while the concentration distribution of Mg exhibited the opposite trend. SEM studies revealed no evidence of intermetallics in the bonding structure. Moreover, no significant single-phase layer is found at the interface for the P1, P2, and P3 samples. For the P4 sample, significant fluctuations in the concentrations of the elements at the interface occur, which are related to the fragmentation of the compounds. Through the analysis of these spectrums, the thickness of the diffusion layer is determined and presented in Figure 4. Specifically, when the hot-pressing strain rate decreased from $1.0 \times 10^{-2} \text{ s}^{-1}$ to $3.3 \times 10^{-4} \text{ s}^{-1}$, there is a steady progression in the thickness of the diffusion layer from $5.7 \mu\text{m}$ to $38.7 \mu\text{m}$.

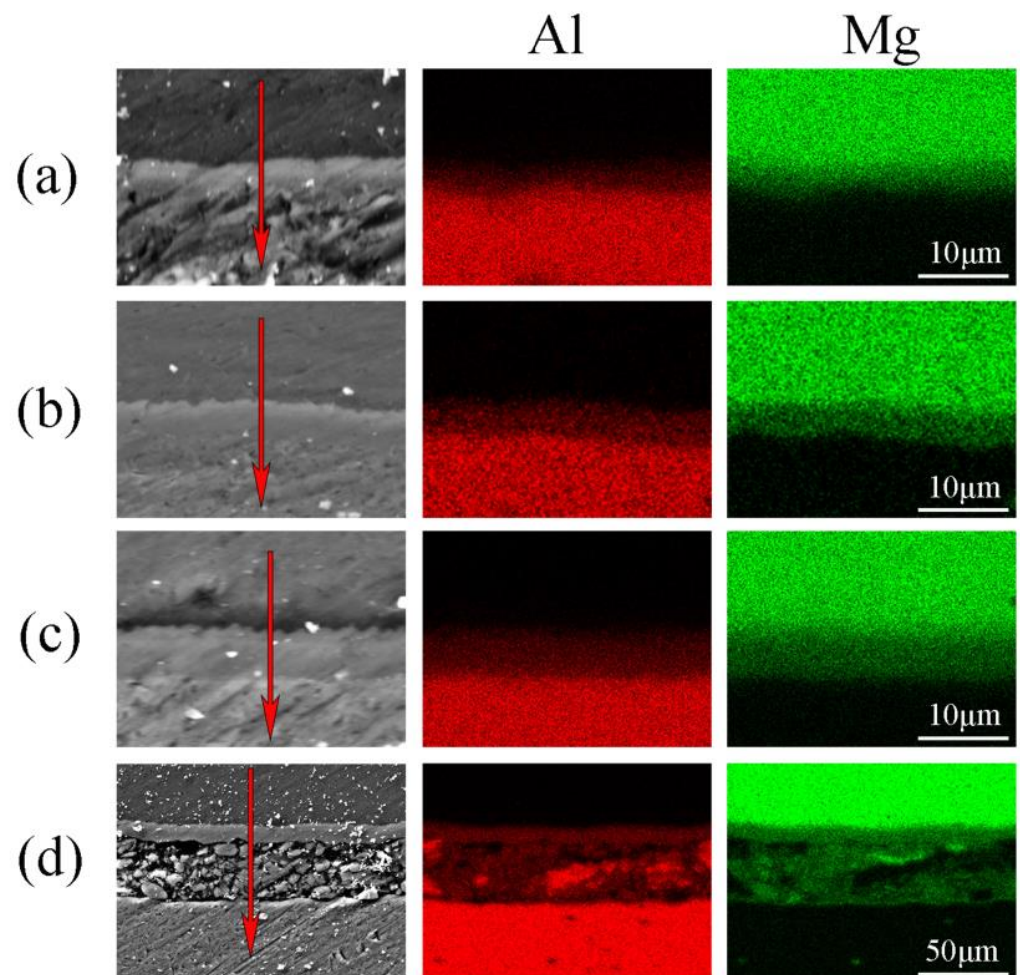


Figure 2. SEM images and accompanying element face-scanning images of (a) the P1 sample, (b) P2 sample, (c) P3 sample, (d) P4 sample. The arrows represent the scanning trajectory of line-scanning in Figure 3.

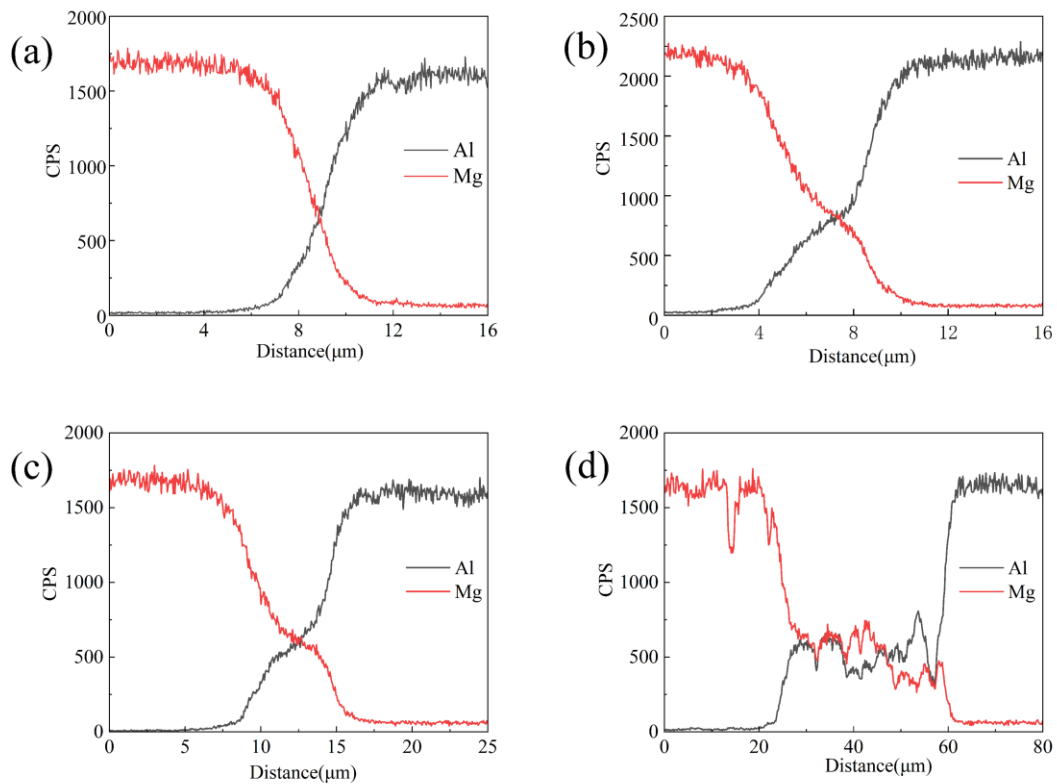


Figure 3. Element line-scanning spectrums of (a) the P1 sample, (b) P2 sample, (c) P3 sample, (d) P4 sample.

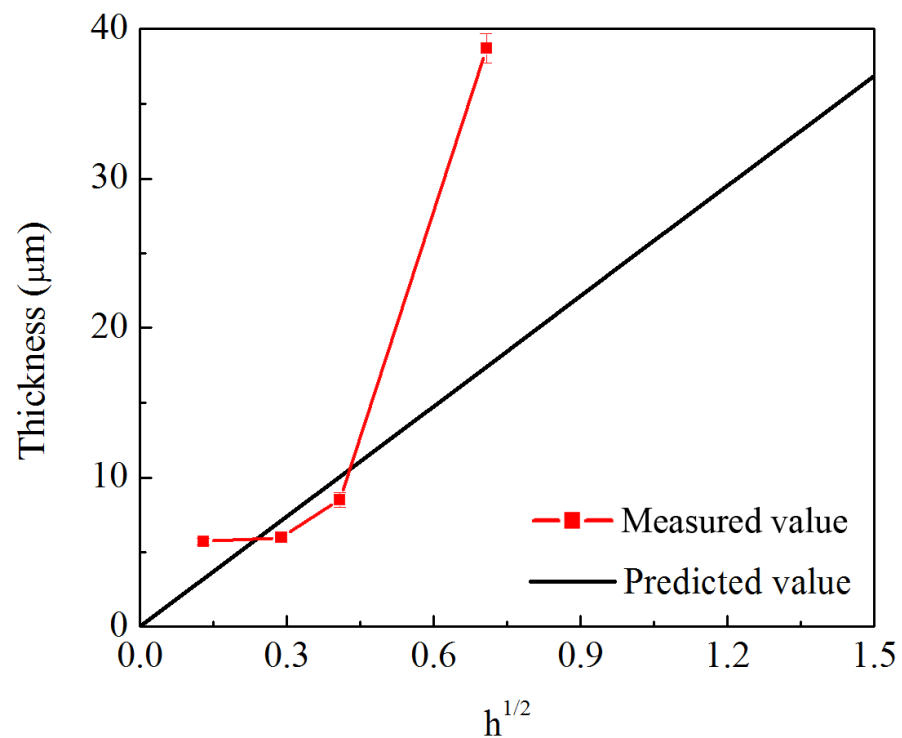


Figure 4. The square root of the annealing time and the intermetallic layer thickness curves.

In the previous work, a linear relationship between the thickness of the compound and the annealing time was reported [30]. Thus, the diffusion mechanism governs the growth of the compounds. In general, the thickness of the intermetallic compound layer

increases linearly with the square root of the holding time. This can be expressed by the following empirical law:

$$y^2 = k_p t$$

where k_p is the growth constant (m^2/s). Wang et al. [31] reported that the growth constant of the diffusion layer at $350\text{ }^\circ\text{C}$ is $1.679 \times 10^{-13}\text{ m}^2/\text{s}$ for a rolled Mg/Al sheet. Based on this, the predicted thickness with holding time is also shown in Figure 4. For the present work, the hot-pressing temperature and strain are constant. Thus, the hot-pressing rate determines the hot-pressing time, as shown in Table 1. It is considered that the hot-pressing time will be the important factor influencing the thickness of the diffusion layer. Figure 4 indicates that with a decreasing hot-pressing rate, the thickness of the diffusion layer gradually deviates from the predicted value. When the strain rate is $3.3 \times 10^{-4}\text{ s}^{-1}$ (corresponding to a hot-pressing time of 30 min), the thickness of the diffusion layer ($38.7\text{ }\mu\text{m}$) is much higher than the predicted value ($17.4\text{ }\mu\text{m}$). Unlike the annealing process, hot pressing imposes high stresses and generates a large strain (40%) during the holding process. Plastic strain might reduce the thickness of the diffusion layer [2]. This indicates that high stress will largely promote inter-diffusion at the interface [32]. Firstly, high bonding pressure increases the contact sites, promoting the diffusion rate and interface reaction [33]. Secondly, crystal defects (e.g., dislocations) via plastic deformation will reduce the activation of the energy of diffusion and enhance the volume diffusion [10,34,35]. Thus, both initial dislocations and plastic strain might accelerate inter-diffusion during hot pressing.

Moreover, previous studies have shown that both high temperatures and prolonged holding times can lead to the formation of Kirkendall holes on the Al side [32]. It is reported that when the annealing temperatures exceed $250\text{ }^\circ\text{C}$, conspicuous Kirkendall voids can be seen at the interface [10]. The emergence of these voids is expected to diminish the overall properties and bonding strength. The primary factor underlying this phenomenon is the discrepancy in diffusion rates between Mg and Al at the interface. Generally, Al exhibits a swifter inter-diffusion rate compared to Mg [36]. Consequently, the surplus vacancies on the Al side eventually facilitate the generation of voids. In this study, no voids appeared at the interface. This may be related to the pressure applied by the hot-pressing process. Hot-pressing deformation can promote inter-diffusion and cause plastic flow of the material, which, in turn, eliminates the voids.

3.2. Phase Compositions at the Interface

Figure 5a displays the positions of EDS points for the P1 samples. The chemical compositions highlighted in Figure 5a can be found in Table 2. Referring to the Al-Mg binary phase diagram (see Figure 5d) at a temperature of $350\text{ }^\circ\text{C}$, the maximum solution of Al in Mg was about $\sim 5\text{ at.}\%$, and the maximum solid solution of Mg in Al was $\sim 10\text{ at.}\%$. Moreover, Mg_2Al_3 (β -phase) and $\text{Mg}_{17}\text{Al}_{12}$ (γ -phase) can be formed at the interface. According to the stoichiometric proportion, it is inferred that position 1 and position 2 are the α -Mg and position 9 is the α -Al. Moreover, abundant LMCs are present between them. Adjacent to the Mg side (position 3–5), the microstructure might be the mixture of α -Mg and $\text{Mg}_{17}\text{Al}_{12}$ LMCs. However, next to the side of the Al (position 8), the mixture of α -Al and Mg_2Al_3 LMCs might be the dominant microstructure. The stoichiometric proportion at position 7 is closer to Mg_2Al_3 LMCs. It also infers that position 6 might contain a mixture of $\text{Mg}_{17}\text{Al}_{12}$ and Mg_2Al_3 . Thus, for the P1 sample, the interface is mostly a multi-phase mixture, and there is no obvious single-phase LMC layer.

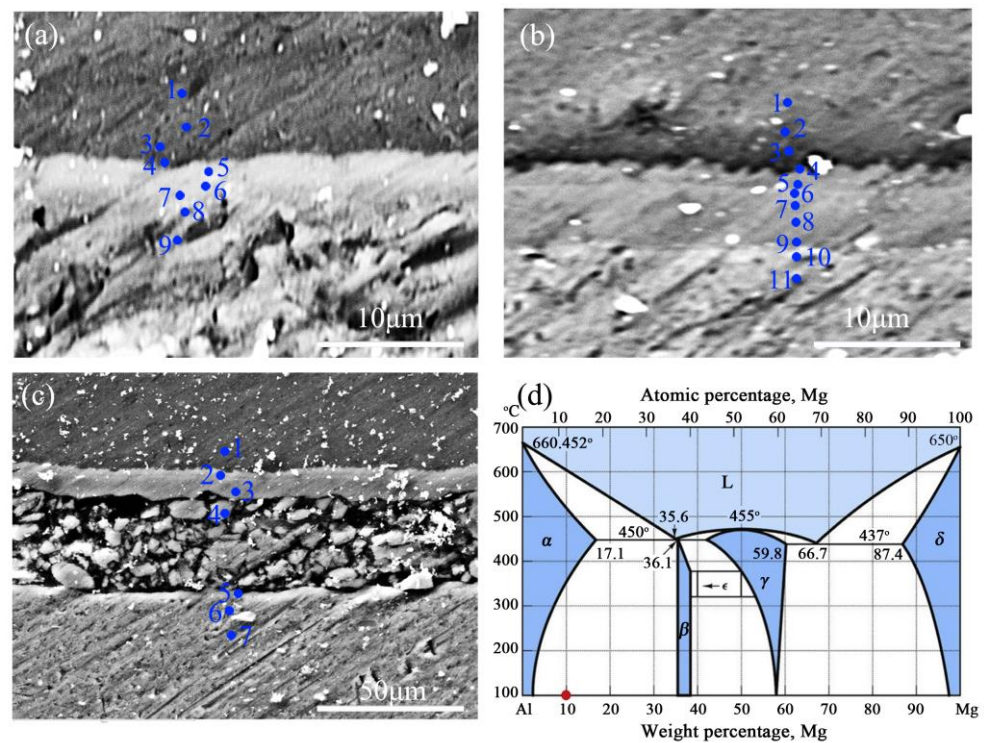


Figure 5. EDS point positions: (a) P1 sample, (b) P3 sample, (c) P4 sample, (d) Mg-Al binary phase diagram (Data form [37]). The numbers in the figures represent the positions of point scan.

Table 2. Chemical composition (at.%) at various positions in Figure 5a.

Position	1	2	3	4	5	6	7	8	9
Mg	97.1	95.3	91.8	86	69.2	51	44.4	21.8	5.7
Al	2.9	4.7	8.2	14	30.8	49	55.6	78.2	94.3
Phase	α -Mg	α -Mg + γ		γ + β			β	β + α -Al	α -Al

Table 3 provides the chemical compositions obtained from various positions at the interface of the P3 sample, as indicated in Figure 5b. Next to the side of the Mg, position 4 has a close chemical composition with $Mg_{17}Al_{12}$ LMCs. However, the composition remains at a very limited width ($<1.5 \mu m$). This indicates that the layer of $Mg_{17}Al_{12}$ is very narrow. In contrast, the interface of the P3 sample contains a relatively thicker single-phase Mg_2Al_3 layer ($\sim 2.4 \mu m$, see positions 6–8). Thus, with decreasing hot-pressing strain, the single-phase LMC layer will be generated at the interface, and the Mg_2Al_3 layer exhibits faster growth than $Mg_{17}Al_{12}$. Table 4 provides the chemical compositions obtained from various positions at the interface of the P4 sample (see Figure 5c). The $Mg_{17}Al_{12}$ layer is still very narrow. However, the width of the Mg_2Al_3 layer reaches $35 \mu m$ (see positions 3–5). Moreover, the EDS results indicate that the broken phase at the interface is mainly Mg_2Al_3 LMCs.

Table 3. Chemical composition (at.%) at various positions in Figure 5b.

Position	1	2	3	4	5	6	7	8	9	10	11
Mg	98.0	93.1	84.2	60.3	45.8	42	38.6	31.9	13.1	5.6	2.9
Al	2.0	6.9	15.8	39.7	54.2	58	61.4	68.1	86.9	94.4	97.1
Phase	α -Mg	α -Mg + γ	γ	γ + β			β		β + α -Al		α -Al

Table 4. Chemical composition (at.%) at various positions in Figure 5c.

Position	1	2	3	4	5	6	7
Mg	97	84.1	40.6	38.6	32.1	3.7	2.7
Al	3	15.9	59.4	61.4	67.9	96.3	97.3
Phase	α -Mg	α -Mg + γ		β			α -Al

Clearly, during the hot-pressing process, extensive inter-diffusion takes place at the interface between Mg and Al. First, Mg and Al supersaturated solid solutions are formed on both sides of the interface. Then, two types of intermetallic compounds, $Mg_{17}Al_{12}$ and Mg_2Al_3 , precipitate within the supersaturated solid solutions of Mg and Al. In the subsequent reaction process, a large number of intermetallic compounds continuously precipitate, forming a single-phase layer. Many studies have proven that the growth constant of Mg_2Al_3 is higher than $Mg_{17}Al_{12}$ [38–40]. Thus, both annealing and thermal processing will generate a thick Mg_2Al_3 layer and a thin $Mg_{17}Al_{12}$ layer. In this work, long-time hot pressing also exhibits a similar phenomenon. Figure 4 indicates that a thick Mg_2Al_3 layer fragmentation occurs during hot pressing. According to the ref. [41], the intermetallic compound layer of the Mg/Al composite sheet is very brittle. The brittle nature of the Mg_2Al_3 phase results in a difficulty of accommodating deformation, and fragmentation occurs during subsequent deformation.

3.3. Shear Strength and Fracture Analysis

For the Mg/Al composite plates as a structural material, preserving structural integrity is of utmost importance. The occurrence of interfacial delamination during operation can result in complete failure. It is reported that a high bonding strength can enhance ductility and tensile strength [10]. Furthermore, when the interface between Mg and Al becomes separated, the Mg matrix loses the protection provided by the Al alloy cladding. Hence, interfacial bond strength serves as a significant gauge for evaluating the quality of composite plates. The interfacial bond strength of composite plates is typically assessed using two methods: the shear test and roller peel test. Here, the shear test using the ASTM D4896 standard [27] was used to evaluate the shear strength. Table 5 displays the shear strengths of the hot-pressed plates. As the strain rate decreases, the shear strength shows an initial increase followed by a decrease. This suggests that the P3 sample demonstrates the maximum shear strength (4.39 MPa).

Table 5. Shear strengths of the hot-pressed Mg-Al samples.

Sample	Shear Strength (MPa)
P1	2.62 ± 0.53
P2	2.47 ± 0.65
P3	4.39 ± 1.22
P4	2.87 ± 1.19

This indicates that the hot-pressing rate can largely influence the shear strength. Hot pressing predominantly creates two types of bonding: mechanical bonding and diffusion bonding [10]. Diffusion bonding is a time-intensive process affected by temperature and stress, while mechanical bonding generates rapidly. Therefore, hot pressing leads to the formation of robust mechanical bonds with uniform flat interfaces and a consistent fixed plastic strain across all samples, and thus the impact of mechanical bonding is believed to be uniform. The restricted hot-pressing time limits extensive inter-diffusion, and a slow hot-pressing speed may encourage heightened interfacial inter-diffusion. As illustrated in Figure 5, a slow hot-pressing rate results in increased compound thickness. Consequently, differences in shear strength are mainly ascribed to discrepancies in metallurgical bond quality. As shown in Figure 2, significant elemental inter-diffusion occurred at the interface

between the substrates and the diffusion layer, and no voids or cracks were generated. This demonstrates that the current hot-pressing process produces effective metallurgical bonding independent of the strain rate. The influence of the strain rate on shear strength might be mainly attributed to the changes in structure, composition, and thickness of the diffusion layer.

As the hot-pressing rate decreases, the thickness of the diffusion layer increases, and the composition of the interface gradually changes from a mixed zone of $Mg_{17}Al_{12}$ and Mg_2Al_3 to two single-phase zones. It is reported that a slight thickening of the diffusion layer improves the bonding strength, and then the bonding strength deteriorates when the thickness of the diffusion layer is greater than $10\ \mu m$ [10]. As shown in Figure 4, the thickness of the diffusion layer is $5.7\ \mu m$, $6\ \mu m$, and $8.5\ \mu m$ for the P1, P2, and P3 samples, respectively. This might be the reason why the P3 sample has higher shear strength. For the P4 sample, the thickness of the diffusion layer is $38.7\ \mu m$, and a thick Mg_2Al_3 single-phase layer can be found. It is reported that the Vickers hardness of the Mg_2Al_3 phase ($\sim 275\ HV$) is always higher than the $Mg_{17}Al_{12}$ phase ($\sim 250\ HV$) [42]. Thus, the Mg_2Al_3 phase exhibits higher hardness and brittleness. The debonding during tension and shear usually occurs at the interface between the Mg_2Al_3 single-phase layer and the Al alloy side [11]. The high brittleness also causes the Mg_2Al_3 single-phase layer to be more susceptible to breakage during processing.

The SEM analysis depicted in Figure 6 provided insights into the shear fracture surfaces of different samples at the Al side. Additionally, the composition of phases on these surfaces was determined through EDS analysis, as outlined in Table 6. The identification of possible phases on the shear fracture surfaces was obtained based on the results of the EDS analysis. The shear fracture interface features of the P1 sample are shown in Figure 6a, and there are distinct granular protrusions at the fracture surface. This infers that the micro-cracks might extend along the grain boundaries during shearing. According to EDS results, the Al side fracture contains a mixed region of the α -Al phase and Mg_2Al_3 phase. As shown in Figure 3 and Table 2, no single-phase layer is formed in the P1 sample. Thus, it infers that the shear fracture took place within the mixed region of Mg_2Al_3 and $Mg_{17}Al_{12}$, which exists between the Mg and Al components.

For the P3 sample, the predominant cleavage river and lamellar structures were prevalent on the fracture surface. The EDS results show the phases on the shear fracture surfaces may be the Mg_2Al_3 phase according to the atomic ratio. This morphology may occur due to the formation of a layer-like single-phase region of intermetallic compounds during the hot-pressing process. Stress is deflected along the Al/ Mg_2Al_3 interface. Since the matrix and the diffusion layer have a strong metallurgical bond, the interface will not fail. Therefore, the stress is further transmitted to the diffusion layer, causing cleavage fracture. Although cleavage fracture is a brittle fracture, the crack has to extend through the interior of the compound grains. Therefore, this type of fracture requires a higher stress than an intergranular fracture. This may explain the high shear strength of the P3 sample.

The shear fracture interface morphology of the P4 sample is shown in Figure 6c, where the fracture surfaces of the Al sides exhibit a mixed feature of granular and fluvial. Moreover, some large bumps and pits can also be found on the fracture surface. EDS results indicate a large amount of Mg_2Al_3 in the phase on both the Mg and Al sides. The results indicate that the fracture occurred in the single-phase Mg_2Al_3 region. As shown in Figure 5, during the hot-pressing process of sample P4, under high temperatures, a thick Mg_2Al_3 layer occurs a certain degree of brittle fracture, and the broken Mg_2Al_3 layer could lead to a decrease in the bonding strength.

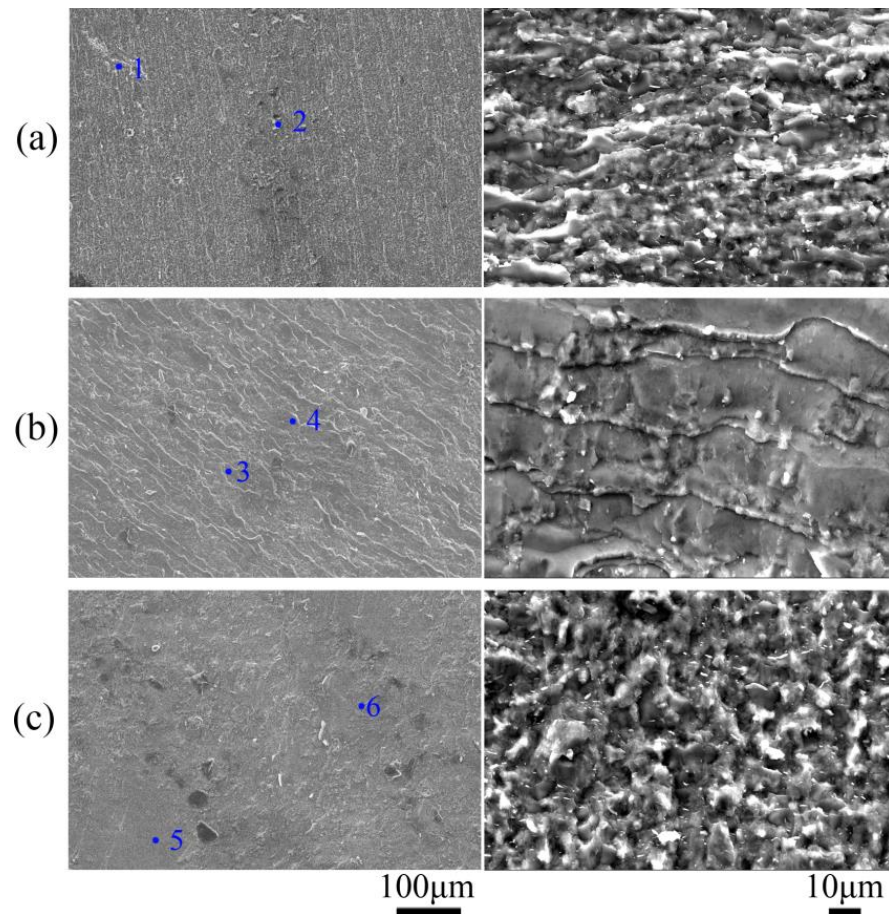


Figure 6. SEM images depicting fracture surfaces on the Al side of the different samples. (a) P1 sample, (b) P3 sample, (c) P4 sample.

Table 6. Chemical composition (at.%) at various positions in Figure 6.

Position	Mg	Al	Possible Phases
1	8.2	91.8	α -Al
2	25.8	74.2	α -Al + β
3	36.1	63.9	β
4	31.2	68.8	α -Al + β
5	40.9	59.1	β
6	26.8	73.2	α -Al + β

To validate the accuracy of the previously mentioned shear fracture position prediction, XRD analysis was conducted on the shear fracture of the P4 sample, as shown in Figure 7. The Al matrix side shear fracture surface (Figure 7a) exhibited the presence of the Al phase and Mg_2Al_3 phase. Similarly, the Mg matrix side shear fracture surface (Figure 7b) revealed the detection of the Mg phase, Mg_2Al_3 phase, and $Mg_{17}Al_{12}$ phase. These XRD results are in line with the findings from the EDS analysis, further confirming that the shear fracture position typically occurs at the Mg_2Al_3 /Al interface and the Mg_2Al_3 layer. The fractured behavior at this position is greatly influenced by the interface structure and the properties of the diffusion layer formed at the Al/Mg interface during hot pressing. It is important to note that intermetallic compounds, such as Mg_2Al_3 and $Mg_{17}Al_{12}$, possess significantly higher Vickers hardness and lower plasticity compared to matrix materials. Additionally, studies have reported that the Vickers hardness of the Mg_2Al_3 phase is higher than $Mg_{17}Al_{12}$ [43]. Consequently, a brittle fracture is more likely to occur in the Mg_2Al_3 phase layer during shear. The thickness of intermetallic compounds also plays a crucial role

in the fracture behavior and shear strength [44], where a thickness exceeding 10 μm results in reduced shear strength. The smooth cleavage plane observed on the shear fracture surface corresponds to the higher shear strength achieved, which explains the highest shear strength exhibited by the P3 sample.

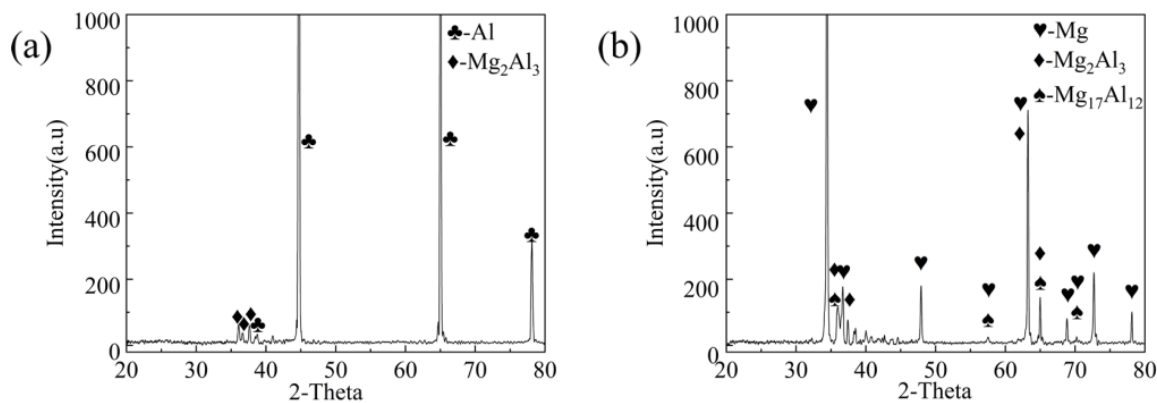


Figure 7. XRD pattern of the shear fracture surfaces in the P4 sample: (a) Al side, (b) Mg side.

It has been shown that rapid hot pressing for a short duration (1 min) and a high strain (40%) under normal conditions can effectively bond AZ31 and 1060. This is contrary to previous methods that required a longer hot-pressing time (>1 h) to achieve sufficient diffusion at the interface. Rapid hot pressing promotes faster diffusion compared to annealing and vacuum diffusion welding [45]. However, a prolonged hot-pressing time (>30 min) may result in the thickening and fragmentation of compounds at the interface, which adversely affects bond strength. Thus, rapid hot pressing prevents compound thickening and enhances processing efficiency. The lack of thickness of the diffusion layer due to rapid hot pressing can also be compensated by subsequent heat treatment. Therefore, rapid hot pressing has the advantage of high efficiency and low cost compared to slow hot pressing.

In addition to the strain rate, the hot-pressing temperature, time, and strain amount also affect the final bond quality and the structure of the interface. Generally, both a high temperature and a long period of time can lead to the thickening of the diffusion layer [10]. The strain amount involves the creation of new surfaces and the evolution of matrix defects, which might also influence the diffusion process [10]. Moreover, the hot-pressing parameters also have a significant influence on the microstructure and texture of the substrates [46]. The interfacial bonding quality and the microstructure of the matrix will jointly affect the overall mechanical properties of the composite sheets [11]. Therefore, the next research phase will focus on developing and optimizing the rapid hot-pressing process. The combined impact of interfacial structure and matrix microstructure on the overall sheet's mechanical properties will be investigated.

4. Conclusions

In this study, a 40% strain hot-pressing test was conducted at 350 $^{\circ}\text{C}$. The effect of the strain rate on the bonding strength and interface structure of the Mg/Al laminated composite plates were studied. The results obtained are summarized as follows:

(1) The Mg/Al composite sheet can be successfully produced through direct hot pressing under atmospheric conditions. A strong inter-diffusion was observed at the Mg/Al interface, and no significant cracks or voids were observed at the interface.

(2) The hot-pressing rate ($3.3 \times 10^{-4} \text{ s}^{-1}$ to $1.0 \times 10^{-2} \text{ s}^{-1}$) will largely affect the interfacial bonding quality and the composition of the interface. As the strain rate decreased, the diffusion layer thickness gradually increased, and the composition of the Mg/Al interface gradually changed from a mixed zone of $\text{Mg}_{17}\text{Al}_{12}$ and Mg_2Al_3 to two single-phase zones.

(3) As the strain rate decreases, there is an initial increase in shear strength followed by a subsequent decrease. The P3 sample demonstrates the highest shear strength of 4.39 MPa, with fracture predominantly occurring within the Mg₂Al₃ layer. When the strain rate of hot pressing reduces to $3.3 \times 10^{-4} \text{ s}^{-1}$, the single-phase zone of Mg₂Al₃ at the interface of the Mg/Al sheet breaks up, resulting the low bond strength.

(4) In this work, only the effects of the hot-pressing rate on interface structure and shear strength were examined. In further work, the effects of the hot-pressing rate on the microstructure of substrates and overall mechanical properties will be investigated. Finally, the overall sheet's mechanical properties will be optimized by synergistically regulating the interfacial structure and microstructure.

Author Contributions: Conceptualization, B.S.; investigation, C.G., B.S., S.T., H.X., M.W. and N.G.; data curation, C.G. and M.W.; writing—original draft preparation, C.G., B.S., S.T., M.W. and T.L.; writing—review and editing, B.S., N.G. and S.G.; project administration, T.L. and S.G. All authors have read and agreed to the published version of the manuscript.

Funding: This work was supported by Fundamental Research Funds for the Central Universities (SWU-XDJH202313), the Chongqing Postdoctoral Science Foundation Funded Project (2112012728014435), the Chongqing Postgraduate Research and Innovation Project (CYS23197), and the Guangdong Major Project of Basic and Applied Basic Research (2020B0301030006).

Data Availability Statement: The data presented in this study are available upon request from the corresponding author. The data are not publicly available due to privacy.

Conflicts of Interest: The authors declare no conflicts of interest.

References

1. Gurau, G.; Gurau, C.; Fernandes, F.M.B.; Alexandru, P.; Sampath, V.; Marin, M.; Galbinas, B.M. Structural Characteristics of Multilayered Ni-Ti Nanocomposite Fabricated by High Speed High Pressure Torsion (HSHT). *Metals* **2020**, *10*, 1629. [\[CrossRef\]](#)
2. Kunčická, L.; Kocich, R. Optimizing electric conductivity of innovative Al-Cu laminated composites via thermomechanical treatment. *Mater. Des.* **2022**, *215*, 110441. [\[CrossRef\]](#)
3. Zhang, X.; Xu, C.; Gao, K.; Liu, B.; Ji, P.; He, J.; Wang, G.; Yin, F. Thickness effect of graphene film on optimizing the interface and mechanical properties of Cu/Ni multilayer composites. *Mater. Sci. Eng. A* **2020**, *798*, 140111. [\[CrossRef\]](#)
4. Peng, H.; Chen, D.; Bai, X.; Wang, P.; Li, D.; Jiang, X. Microstructure and mechanical properties of Mg-to-Al dissimilar welded joints with an Ag interlayer using ultrasonic spot welding. *J. Magnes. Alloy.* **2020**, *8*, 552–563. [\[CrossRef\]](#)
5. Zhu, C.; Xu, S.; Gao, W.; Meng, Y.; Lin, S.; Dai, L. Microstructure characteristics and mechanical properties of Al/Mg joints manufactured by magnetic pulse welding. *J. Magnes. Alloy.* **2021**, *11*, 2366–2375. [\[CrossRef\]](#)
6. Qin, L.; Fan, M.; Guo, X.; Tao, J. Plastic deformation behaviors of Ti-Al laminated composite fabricated by vacuum hot-pressing. *Vacuum* **2018**, *155*, 96–107. [\[CrossRef\]](#)
7. Bai, S.; Liu, L.; Li, K.; Jiang, B.; Huang, G.; Zhang, D.; Pan, F. Investigation into the microstructure, tensile properties and bendability of Mg–Al–Zn/Mg-xGd laminated composite sheets extruded by porthole die. *J. Mater. Res. Technol.* **2022**, *21*, 12–29. [\[CrossRef\]](#)
8. Bai, S.; Wei, L.; He, C.; Liu, L.; Dong, Z.; Liu, W.; Jiang, B.; Huang, G.; Zhang, D.; Xu, J. Effects of layer thickness ratio on the bendability of Mg-Al-Zn/Mg-Gd laminated composite sheet. *J. Mater. Res. Technol.* **2022**, *21*, 1013–1028. [\[CrossRef\]](#)
9. Bi, X.; Hu, Y.; Li, R.; Zhao, H.; Li, T. A novel method for preparing Al/Mg/Al laminated composite material, processing maps and interface diffusion analysis. *J. Alloys Compd.* **2022**, *900*, 163417. [\[CrossRef\]](#)
10. Liu, T.; Song, B.; Huang, G.; Jiang, X.; Guo, S.; Zheng, K.; Pan, F. Preparation, structure and properties of Mg/Al laminated metal composites fabricated by roll-bonding, a review. *J. Magnes. Alloy.* **2022**, *10*, 2062–2093. [\[CrossRef\]](#)
11. Yu, Z.; Wang, T.; Liu, C.; Ma, Y.; Liu, W. Investigation on microstructure, mechanical properties and fracture mechanism of Mg/Al laminated composites. *Mater. Sci. Eng. A* **2022**, *848*, 143410. [\[CrossRef\]](#)
12. Prasad, S.V.S.; Prasad, S.B.; Verma, K.; Mishra, R.K.; Kumar, V.; Singh, S. The role and significance of Magnesium in modern day research-A review. *J. Magnes. Alloy.* **2022**, *10*, 1–61. [\[CrossRef\]](#)
13. Xu, W.; Birbilis, N.; Sha, G.; Wang, Y.; Daniels, J.E.; Xiao, Y.; Ferry, M. A high-specific-strength and corrosion-resistant magnesium alloy. *Nat. Mater.* **2015**, *14*, 1229–1235. [\[CrossRef\]](#) [\[PubMed\]](#)
14. Rooy, E.L.; Committee, A.H. Introduction to Aluminum and Aluminum Alloys. In *Properties and Selection: Nonferrous Alloys and Special-Purpose Materials*; ASM International: Almere, The Netherlands, 1990.
15. Zeng, Y.; Gong, J. The trajectory optimization of spray painting robot for conical surface. *Adv. Mater. Res.* **2010**, *139*, 2189–2194. [\[CrossRef\]](#)

16. Guan, F.; Jiang, W.; Li, G.; Zhu, J.; Wang, J.; Jie, G.; Fan, Z. Effect of vibration on interfacial microstructure and mechanical properties of Mg/Al bimetal prepared by a novel compound casting. *J. Magnes. Alloy.* **2022**, *10*, 2296–2309. [[CrossRef](#)]
17. Zhang, N.; Wang, W.; Cao, X.; Wu, J. The effect of annealing on the interface microstructure and mechanical characteristics of AZ31B/AA6061 composite plates fabricated by explosive welding. *Mater. Des. (1980–2015)* **2015**, *65*, 1100–1109. [[CrossRef](#)]
18. Zhang, X.; Castagne, S.; Yang, T.; Gu, C.; Wang, J. Entrance analysis of 7075 Al/Mg–Gd–Y–Zr/7075 Al laminated composite prepared by hot rolling and its mechanical properties. *Mater. Des.* **2011**, *32*, 1152–1158. [[CrossRef](#)]
19. Kumar, P.; Ghosh, S.K.; Saravanan, S.; Barma, J.D. Significance of the Interlayer in Explosive Welding of Similar and Dissimilar Materials: Review. *Combust. Explos. Shock. Waves* **2023**, *59*, 253–278. [[CrossRef](#)]
20. Song, J.; She, J.; Chen, D.; Pan, F. Latest research advances on magnesium and magnesium alloys worldwide. *J. Magnes. Alloy.* **2020**, *8*, 1–41. [[CrossRef](#)]
21. Zhu, B.; Liang, W.; Li, X. Interfacial microstructure, bonding strength and fracture of magnesium–aluminum laminated composite plates fabricated by direct hot-pressing. *Mater. Sci. Eng. A* **2011**, *528*, 6584–6588. [[CrossRef](#)]
22. Loh, N.; Sia, K. An overview of hot isostatic pressing. *J. Mater. Process. Technol.* **1992**, *30*, 45–65. [[CrossRef](#)]
23. Liu, T.; Guo, C.; Tan, S.; Song, B.; Wang, M.; Huang, G.; Zheng, K.; Pan, F. Effect of Hot-Pressing Rate on Interface and Bonding Strength of Mg/Al Composite Sheets with Zn Interlayer. *J. Mater. Eng. Perform.* **2023**, 1–12. [[CrossRef](#)]
24. Cao, M.; Deng, K.-K.; Nie, K.-B.; Wang, C.-J.; Wang, L.; Liang, W. Microstructure, mechanical properties and formability of Ti/Al/Ti laminated composites fabricated by hot-pressing. *J. Manuf. Process.* **2020**, *58*, 322–334. [[CrossRef](#)]
25. Mirzadeh, H. High strain rate superplasticity via friction stir processing (FSP): A review. *Mater. Sci. Eng. A* **2021**, *819*, 141499. [[CrossRef](#)]
26. Li, X.; Xia, W.; Yan, H.; Chen, J.; Su, B.; Song, M.; Li, Z.; Li, Y. Dynamic recrystallization behaviors of high Mg alloyed Al-Mg alloy during high strain rate rolling deformation. *Mater. Sci. Eng. A* **2019**, *753*, 59–69. [[CrossRef](#)]
27. Wang, Y.; Rao, M.; Li, L.; Luo, G.; Shen, Q.; Zhang, L. Accelerated bonding of magnesium and aluminum with a CuNi/Ag/CuNi sandwich interlayer by plasma-activated sintering. *Metall. Mater. Trans. A* **2016**, *47*, 631–636. [[CrossRef](#)]
28. Budhe, S.; Banea, M.; De Barros, S.; Da Silva, L. An updated review of adhesively bonded joints in composite materials. *Int. J. Adhes. Adhes.* **2017**, *72*, 30–42. [[CrossRef](#)]
29. Zhang, X.; Yang, T.; Castagne, S.; Gu, C.; Wang, J. Proposal of bond criterion for hot roll bonding and its application. *Mater. Des.* **2011**, *32*, 2239–2245. [[CrossRef](#)]
30. Tanaka, Y.; Kajihara, M.; Watanabe, Y. Growth behavior of compound layers during reactive diffusion between solid Cu and liquid Al. *Mater. Sci. Eng. A* **2007**, *445*, 355–363. [[CrossRef](#)]
31. Wang, P.; Chen, Z.; Hu, C.; Li, B.; Mo, T.; Liu, Q. Effects of annealing on the interfacial structures and mechanical properties of hot roll bonded Al/Mg clad sheets. *Mater. Sci. Eng. A* **2020**, *792*, 139673. [[CrossRef](#)]
32. Mahendran, G.; Babu, S.; Balasubramanian, V. Analyzing the effect of diffusion bonding process parameters on bond characteristics of Mg–Al dissimilar joints. *J. Mater. Eng. Perform.* **2010**, *19*, 657–665. [[CrossRef](#)]
33. Elsa, M.; Khorram, A.; Ojo, O.O.; Paidar, M. Effect of bonding pressure on microstructure and mechanical properties of aluminum/copper diffusion-bonded joint. *Sādhanā* **2019**, *44*, 126. [[CrossRef](#)]
34. Oh-Ishi, K.; Edalati, K.; Kim, H.S.; Hono, K.; Horita, Z. High-pressure torsion for enhanced atomic diffusion and promoting solid-state reactions in the aluminum–copper system. *Acta Mater.* **2013**, *61*, 3482–3489. [[CrossRef](#)]
35. Varmazyar, J.; Khodaei, M. Diffusion bonding of aluminum–magnesium using cold rolled copper interlayer. *J. Alloys Compd.* **2019**, *773*, 838–843. [[CrossRef](#)]
36. Kulkarni, K.N.; Luo, A.A. Interdiffusion and phase growth kinetics in magnesium–aluminum binary system. *J. Phase Equilibria Diffus.* **2013**, *34*, 104–115. [[CrossRef](#)]
37. Jafarian, M.; Khodabandeh, A.; Manafi, S. Evaluation of diffusion welding of 6061 aluminum and AZ31 magnesium alloys without using an interlayer. *Mater. Des. (1980–2015)* **2015**, *65*, 160–164. [[CrossRef](#)]
38. Vrtnik, S.; Jazbec, S.; Jagodič, M.; Korelec, A.; Hosnar, L.; Jagličić, Z.; Jeglič, P.; Feuerbacher, M.; Mizutani, U.; Dolinšek, J. Stabilization mechanism of γ -Mg₁₇Al₁₂ and β -Mg₂A₁₃ complex metallic alloys. *J. Phys. Condens. Matter* **2013**, *25*, 425703. [[CrossRef](#)]
39. Zheng, B.; Zhao, L.; Hu, X.; Dong, S.; Li, H. First-principles studies of Mg₁₇Al₁₂, Mg₂A₁₃, Mg₂Sn, MgZn₂, Mg₂Ni and Al₁₃Ni phases. *Phys. B Condens. Matter* **2019**, *560*, 255–260. [[CrossRef](#)]
40. Zhou, Y.; Zhu, Y.; Zhu, Y.; Li, L. Phase transformation, kinetics and thermodynamics during the combustion synthesis of Mg₂A₁₃ alloy. *J. Alloys Compd.* **2015**, *628*, 257–262. [[CrossRef](#)]
41. Li, G.; Jiang, W.; Guan, F.; Zhu, J.; Zhang, Z.; Fan, Z. Microstructure, mechanical properties and corrosion resistance of A356 aluminum/AZ91D magnesium bimetal prepared by a compound casting combined with a novel Ni–Cu composite interlayer. *J. Mater. Process. Technol.* **2021**, *288*, 116874. [[CrossRef](#)]
42. Spencer, K.; Zhang, M.X. Heat treatment of cold spray coatings to form protective intermetallic layers. *Scr. Mater.* **2009**, *61*, 44–47. [[CrossRef](#)]
43. Yang, H.; Guo, X.; Wu, G.; Wang, S.; Ding, W. Continuous intermetallic compounds coatings on AZ91D Mg alloy fabricated by diffusion reaction of Mg–Al couples. *Surf. Coat. Technol.* **2011**, *205*, 2907–2913. [[CrossRef](#)]
44. Lee, K.S.; Yoon, D.H.; Kim, H.K.; Kwon, Y.-N.; Lee, Y.-S. Effect of annealing on the interface microstructure and mechanical properties of a STS–Al–Mg 3-ply clad sheet. *Mater. Sci. Eng. A* **2012**, *556*, 319–330. [[CrossRef](#)]

45. Harrigan, W.C. Commercial processing of metal matrix composites. *Mater. Sci. Eng. A* **1998**, *244*, 75–79. [[CrossRef](#)]
46. Zhao, K.; Xu, D.; Li, H.; Zhang, J.; Chen, D. Microstructure and mechanical properties of Mg/Mg bimetal composites fabricated by hot-pressing diffusion and co-extrusion. *Mater. Sci. Eng. A* **2019**, *764*, 138194. [[CrossRef](#)]

Disclaimer/Publisher's Note: The statements, opinions and data contained in all publications are solely those of the individual author(s) and contributor(s) and not of MDPI and/or the editor(s). MDPI and/or the editor(s) disclaim responsibility for any injury to people or property resulting from any ideas, methods, instructions or products referred to in the content.